Bioactive Materials 25 (2023) 640–656

Contents lists available at ScienceDirect

Bioactive Materials

journal homepage: www.keaipublishing.com/en/journals/bioactive-materials

MiRNA 24-3p-rich exosomes functionalized DEGMA-modified hyaluronic acid hydrogels for corneal epithelial healing

Xiaomin Sun [a,b,c,d,e], Wenjing Song [a,b,c,d,e,*], Lijing Teng [i], Yongrui Huang [a,b,c,d,e], Jia Liu [a,b,c,d,e], Yuehai Peng [b,c,d,e,f], Xiaoting Lu [b,c,d,e,f], Jin Yuan [j], Xuan Zhao [j], Qi Zhao [a,b,c,d,e], Yingni Xu [a,b,c,d,e], Jingjie Shen [a,b,c,d,e], Xiaoyun Peng [a,b,c,d,e], Li Ren [a,b,c,d,e,g,h,**]

[a] School of Materials Science and Engineering, South China University of Technology, Guangzhou, 510006, China
[b] National Engineering Research Center for Tissue Restoration and Reconstruction, Guangzhou, 510006, China
[c] Key Laboratory of Biomedical Engineering of Guangdong Province, South China University of Technology, Guangzhou, 510006, China
[d] Key Laboratory of Biomedical Materials and Engineering of the Ministry of Education, South China University of Technology, Guangzhou, 510006, China
[e] Innovation Center for Tissue Restoration and Reconstruction, South China University of Technology, Guangzhou 510006, China
[f] School of Biological Science and Engineering, South China University of Technology, Guangzhou, 510006, China
[g] Sino-Singapore International Joint Research Institute, Guangzhou, 510555, China
[h] Bioland Laboratory (Guangzhou Regenerative Medicine and Health Guangdong Laboratory), Guangzhou, 510005, China
[i] School of Biology and Engineering, Guizhou Medical University, Guiyang, Guizhou, 550025, China
[j] State Key Laboratory of Ophthalmology, Zhongshan Ophthalmic Center, Sun Yat-sen University, Guangzhou, 510623, China

ARTICLE INFO

Keywords:
miRNA 24-3p
Exosome
Corneal epithelium
Cell migration
Thermosensitive hydrogel

ABSTRACT

The damage of corneal epithelium may lead to the formation of irreversible corneal opacities and even blindness. The migration rate of corneal epithelial cells directly affects corneal repair. Here, we explored ocu-microRNA 24-3p (miRNA 24-3p) that can promote rabbit corneal epithelial cells migration and cornea repair. Exosomes, an excellent transport carrier, were exacted from adipose derived mesenchymal stem cells for loading with miRNA 24-3p to prepare miRNA 24-3p-rich exosomes (Exos-miRNA 24-3p). It can accelerate corneal epithelial migration *in vitro* and *in vivo*. For application in cornea alkali burns, we further modified hyaluronic acid with di(ethylene glycol) monomethyl ether methacrylate (DEGMA) to obtain a thermosensitive hydrogel, also reported a thermosensitive DEGMA-modified hyaluronic acid hydrogel (THH) for the controlled release of Exos-miRNA 24-3p. It formed a highly uniform and clear thin layer on the ocular surface to resist clearance from blinking and extended the drug–ocular–epithelium contact time. The use of THH-3/Exos-miRNA 24-3p for 28 days after alkali burn injury accelerated corneal epithelial defect healing and epithelial maturation. It also reduced corneal stromal fibrosis and macrophage activation. MiRNA 24-3p-rich exosomes functionalized DEGMA-modified hyaluronic acid hydrogel as a multilevel delivery strategy has a potential use for cell-free therapy of corneal epithelial regeneration.

1. Introduction

Corneal epithelium acts as a mechanical barrier to maintain corneal homeostasis. In daily life, corneal epithelium damage under mechanical force, ocular trauma, and chemical injury can often lead to the formation of irreversible corneal opacities and even blindness [1,2]. Once the corneal epithelium and basement membrane are destroyed, the surrounding corneal epithelial cells secrete various cytokines, chemokines, and growth factors [3], activate fibroblasts to differentiate into myofibroblasts, and cause corneal opacity and blindness [4]. The common clinical treatments for the healing of corneal epithelium include antibiotics, hormones, wearing contact lenses, amniotic membrane covering, and transplantation. [5–8] The drug treatment exhibits certain effects, but it has tolerance and side effects [9–12], such as injury of retina and optic nerve. Therefore, a therapeutic strategy that allows

Peer review under responsibility of KeAi Communications Co., Ltd.
* Corresponding author.
** Corresponding author.
E-mail addresses: phsongwj@scut.edu.cn (W. Song), psliren@scut.edu.cn (L. Ren).

https://doi.org/10.1016/j.bioactmat.2022.07.011
Received 25 April 2022; Received in revised form 7 July 2022; Accepted 9 July 2022
Available online 15 July 2022

rapid corneal epithelium wound healing is urgently required.

In tissue regeneration, exosomes with a diameter of 30–200 nm secretion by mesenchymal stem cells (MSCs) have attracted extensive attention. They contain proteins, lipids and RNAs [13] and have become increasingly important medium for intercellular communication [14]. Many functions of exosomes are mediated by its encapsulated microRNAs (miRNAs). MiRNAs are small non-coding RNAs that can result in gene silencing. In transportation system, miRNAs cannot directly enter cells, so it must rely on transport carriers to enter target cells. Scholars have done a lot of research on micro/nano structure carriers and used them to transport nucleic acid, such as tetrahedral framework nucleic acids [15–17] and exosomes. Exosomes as a natural material have biosafety and absent of immunogenicity [18,19]. It are the most potential transportation carrier at present, and have been commercialized by many biological companies [20,21].

Abbreviations

TEM	Transmission Electron Microscopy
NanoFCM	Nanoparticle Flow Cytometry
NTA	Nanoparticle Tracking Analysis
WB	Western Blot
HSP 70	70 Kilodalton Heat Shock Proteins
CDC42	Cell Division Control Protein 42 Homolog
FRS2	Fibroblast Growth Factor Receptor Substrate 2
CTGF	Connective Tissue Growth Factor
EGFR	Epidermal Growth Factor Receptor
MMP9	Matrix Metallopeptidase 9
qRT-PCR	Real-Time Quantitative Reverse Transcription PCR
MiRNA NC	MicroRNA Negative Control
CK3	Cytokeratin 3
ZO-1	Zonula Occludens-1
α-SMA	Alpha Smooth Muscle Actin
MAPK	Mitogen-activated Protein Kinase

Corneal epithelium in all exposed epithelial surfaces has an innate protective mechanism that hinders efficient drug delivery to the eye, which should be considered in corneal epithelial therapy [22–25]. Through traditional eye drop administration, only a small part of the effective ingredients is usually absorbed but most of them are cleaned by the blinking of the eyelids frequently before flowing into the nasolacrimal duct [25]. Increasing the frequency of eye-drop doses per day can improve local dosage, but it results in potential risks of ocular surface irritation and systemic side effects (such as metabolic disorder), while patient compliance to the treatment regimen decreases [26,27]. Therefore, approaches towards more efficient, longer-lasting, and safer topical ocular exosome delivery should be developed.

In the present study, we investigated adipose derived mesenchymal stem cells (ADSCs)-derived exosomes (Exos) and miRNA 24-3p effects on the biological properties of corneal epithelial cells. Cooperating with the advantages of Exos (anti-inflammatory, cell proliferation and migration) and miRNAs 24-3p (cell migration), we prepared miRNA 24-3p-modified exosomes (Exos-miRNA 24-3p) for corneal epithelial wound repair. Furthermore, based on the complexity and severity of corneal alkali burn, we designed and developed a thermosensitive hyaluronic acid hydrogel modified with di(ethylene glycol) monomethyl ether methacrylate (DEGMA) delivered miRNA 24-3p-rich exosomes (Exos-miRNA 24-3p) for corneal epithelial defect healing. We evaluated the efficacy of this delivery system in an animal model of alkali burns. The delivery system provided a promising therapeutic strategy for corneal epithelial healing and treatment of ocular surface diseases.

2. Materials and methods

See Supporting Information.

3. Results

3.1. Identification of ADSCs-derived exosomes

ADSCs extracted from rabbit groin were identified by morphological observation and marker proteins (Fig. S1). To identify the quality of Exos, we analysed the morphology, particle size, concentration and marker proteins of Exos by TEM, NanoFCM, NTA and WB, respectively (Fig. 1). The obtained Exos showed a saucer shape and small vesicles with depression in the middle, which are consistent with previous results (Fig. 1a). The result of aggregated distribution may be caused by high-density or insufficient resuspension during sample preparation. The marker proteins (CD 9, CD 81 and Flotillin 1) of Exos were over expressed, while for that of ADSCs, CD 81 was not expressed, and CD 9 and Flotillin-1 had a low expression for the identification of extracellular vesicles, as shown in Fig. 1b. HSP 70 was highly expressed in ADSCs, but not in Exos. The size distribution of Exos was tested using NTA and NanoFCM (Fig. 1c and **d**). The size distribution (40–150 nm; mean = 72.41 nm) of Exos measured by NanoFCM was smaller than that of NTA (30–200 nm; mean = 125 nm) and was in good agreement with the results of TEM. In addition, the concentration of Exos tested by NanoFCM was 100–1000 times higher than that tested by NTA. In the present work, the concentration unit for Exos was μg/mL (1 μg ≈ 5.1×10^5 particles). Therefore, NanoFCM is suitable as an instrument to detect the size distribution and concentration of Exos. After co-culture of Exos with rabbit corneal epithelial cells (RCECs) for 24 h, Exos successfully entered RCECs, indicating that Exos were easily endocytosed or internalised by RCECs (Fig. 1e).

3.2. Biological functions of ADSCs-derived exosomes

After proving that Exos easily entered RCECs, the biological function of Exos on RCECs were studied by treatment with different concentrations of Exos. As shown in Fig. 2a and b, cell migration increased with the increase of Exos concentration at 12 or 24 h. At 24 h, Exos with a concentration of 20 μg/mL mediated the complete closure of cell wound caused by the migration of RCECs, and this observation was significantly different from those of other groups ($p \leq 0.001$). The effect of Exos on the proliferation of RCECs was also studied (Fig. 2c). On the first day, all experimental groups had no difference on RCEC proliferation compared with the control group ($p > 0.05$). On the third day, Exos with a concentration of 20 μg/mL had a significant effect on RCEC proliferation compared with the control group ($p \leq 0.05$). On the fifth day, the cell proliferation increased with the increase of Exos concentration, and significant differences were observed between the experimental groups and control group ($p \leq 0.05$), and it showed an obvious growth trend. Cell chemotaxis also represents a kind of cell migration ability. Different concentrations of Exos were added to the lower chamber of Transwell to induce RCECs in the upper chamber to pass through (Fig. 2d and e). The same as the results of cell migration, the cell chemotaxis became more obvious with the increase of Exos concentration. The number of cells induced to pass through the chamber was significantly higher than that in the control group (only medium, Exos free) when the concentration of Exos was 10 or 20 μg/mL ($p \leq 0.001$), as indicated in Fig. 2e. The effect of different concentrations of Exos on vinculin expression from RCECs was also studied (Fig. 2f and g). The expression of vinculin gradually increased with the increase of Exos concentration from the results in Fig. 2g. The expression ratios of vinculin were more than 95% when the concentrations of Exos was more than 20 μg/mL. Significant differences were observed between the 10 or 20 μg/mL group and the control group ($p \leq 0.01$). Finally, the regulatory effect of different concentrations of Exos on migration-related genes was studied by qRT-PCR (Fig. 2h). In

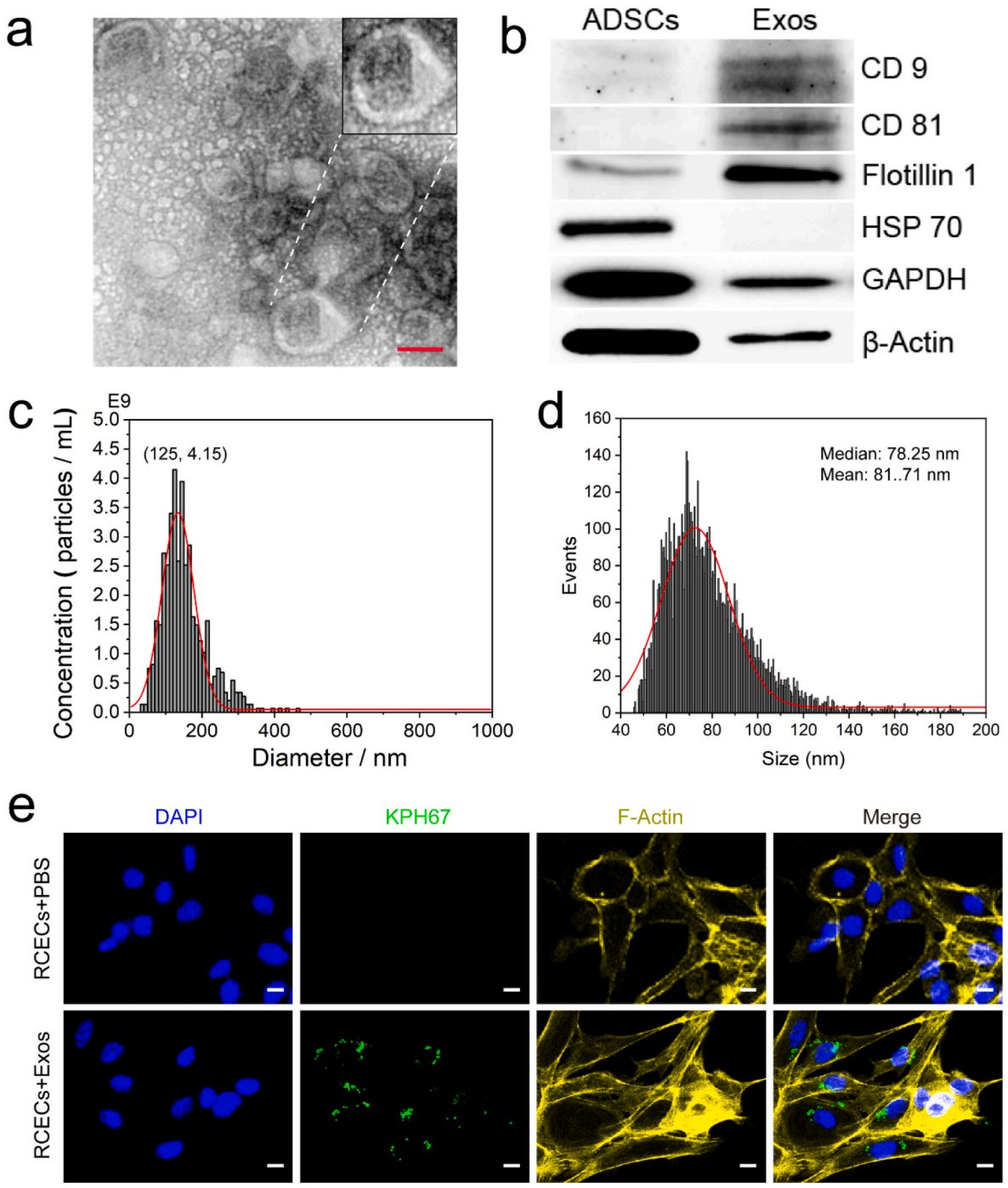

Fig. 1. Identification of Exos. (a) Representative TEM image of Exos. Scale bar: 50 nm. (b) Presence of marker proteins of Exos (CD9, CD 81, Flotillin 1 and HSP 70). (c and d) Size distribution of Exos. c is the result of NTA; d is the result of NanoFCM. (e) Uptake of Exos by RCECs. The concentration of Exos is 20 μg/mL. Scale bar: 10 μm.

the expression of CDC42 gene, the expression of gene was slightly up-regulated with the increase of Exos concentration, but significant differences were observed ($p \leq 0.01$). In the FRS2 and CTGF gene, the upregulation of gene was not affected by the concentration of Exos, but they were different from control group. More importantly, the expression of EGFR and MMP9 gene was significantly up-regulated with the increase of Exos concentration. Therefore, the following work focuses on the study of EGFR and MMP9 proteins.

3.3. RCEC proliferation and migration by MiRNA 24-3p

MiRNA 24-3p has been reported to regulate cancer cell migration [28–30]. The majority of cancer cells are epithelial in origin, beginning in a tissue that lines the inner or outer surfaces of the body. Thus, we hypothesized that miRNA 24-3p has the same migration effect on corneal epithelial cells. The hypothesis that miRNA 24-3p also can regulate corneal epithelial cell migration was verified in Fig. 3. It was observed that miRNA 24-3p was overexpressed in ADSCs but not or low expressed in Exos and RCECs through the small-RNA sequencing of ADSCs, RCECs and Exos (Fig. 3a). To verify the regulatory effect of

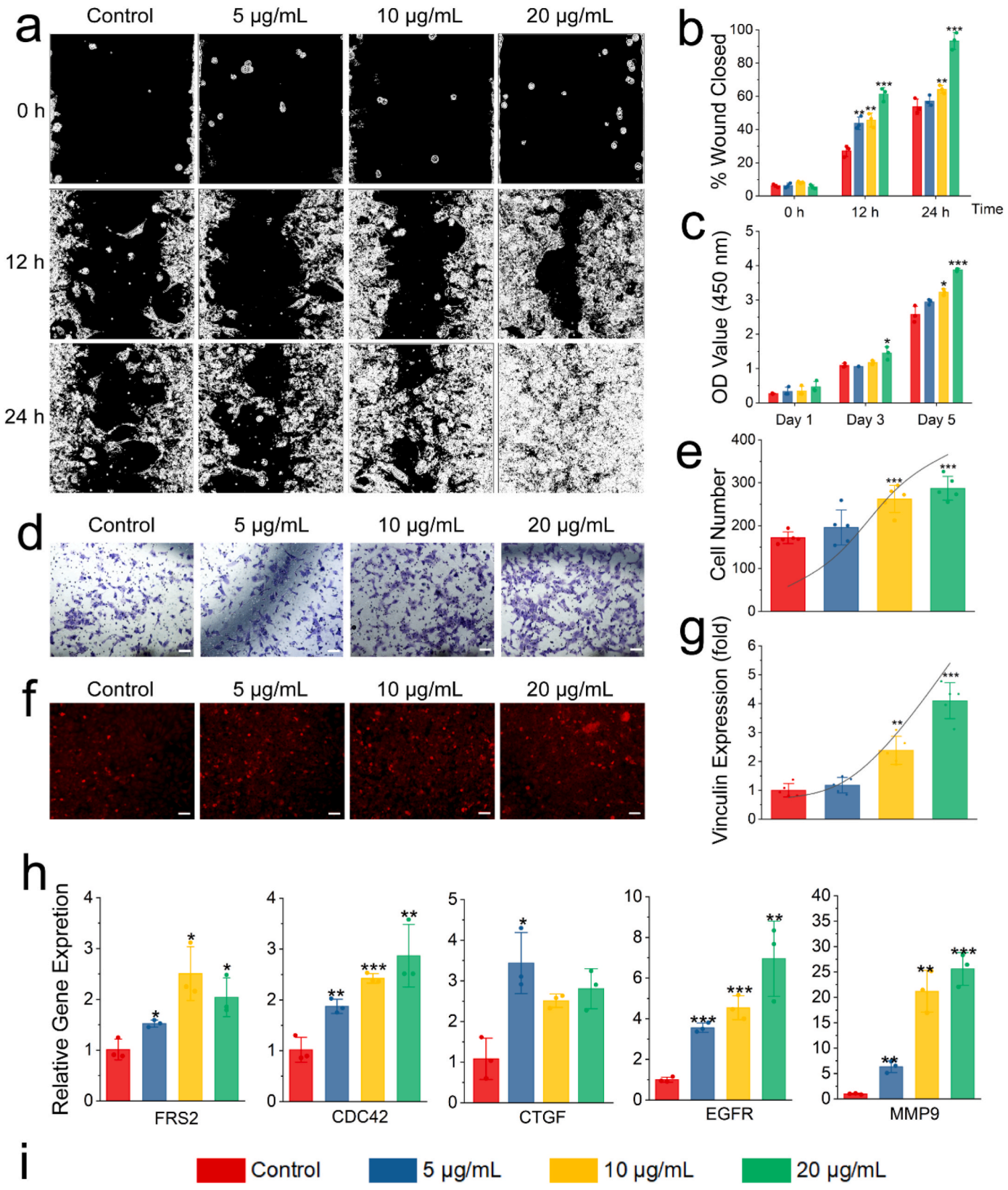

Fig. 2. Biological functions of Exos. (a) The cell wound models *in vitro* by the ibidi Culture-Insert 2 well. (b) Quantitative evaluation of the cell wound by ImageJ. (c) Cell proliferation of different concentrations of Exos on RCECs by CCK-8. (d) Chemotaxis of RCECs by Transwell assay. Scale bar: 100 μm. (e) Cell number passing through Transwell on cell chemotaxis test. (f) Expression of vinculin with different concentrations of Exos on RCECs. Scale bar: 100 μm. (g) Semiquantitative evaluation of the expression of vinculin using ImageJ. (h) Expression of cell migration-related genes, including FRS2, CDC42, CTGF, EGFR and MMP9, on day 1. (i) Concentration of exosomes indicated by columns of different colours in the figures. *p ≤ 0.05, **p ≤ 0.01 and ***p ≤ 0.001 for control.

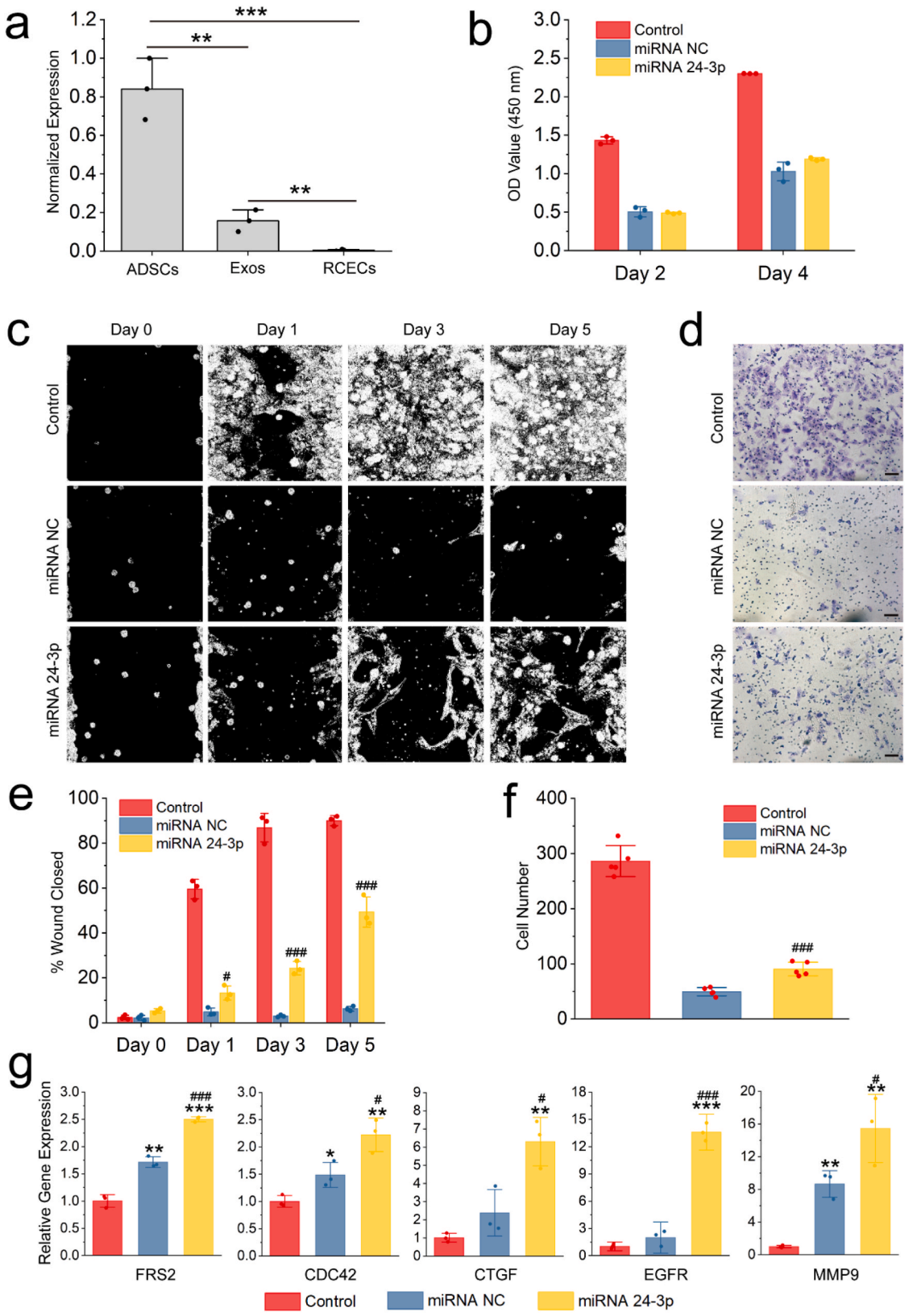

Fig. 3. RCEC proliferation and migration by miRNA 24-3p. (a) The level of expression via normalization after small-RNA sequencing of RCECs, ADSCs and Exos (n = 3). **p ≤ 0.01 and ***p ≤ 0.001. (b) Cell proliferation of miRNA 24-3p on RCECs using CCK-8 (n = 3). (c) *In vitro* wound experiment of miRNA 24-3p. The cell wound models *in vitro* were established using the ibidi Culture-Insert 2 Well. The original images were thresholded using ImageJ for easy observation. (d) Effect of miRNA 24-3p on chemotaxis of RCECs by Transwell. Scale bar: 100 μm. (e) Quantitative evaluation of the cell wound using ImageJ. (f) Cell number passing through Transwell in an environment with miRNA 24–3. (g) Expression of FRS2, CDC42, CTGF, EGFR and MMP9 1 day after transfection. *p ≤ 0.05, **p ≤ 0.01 and ***p ≤ 0.001 for control; #p ≤ 0.05, ##p ≤ 0.01 and ###p ≤ 0.001 for miRNA NC (e, g and f).

miRNA 24-3p on biological functions of RCECs, we performed cell proliferation (Fig. 3b), cell wound healing (Fig. 3c and e), cell chemotaxis (Fig. 3d and f) and qRT-PCR (Fig. 3g) tests. After miRNA transfection by lipofectamine RNAiMAX (a commercialized transfection reagent), cell proliferation, cell chemotaxis and cell migration were significantly reduced compared with control group (native RCECs), indicating that the transfection reagent has certain cytotoxicity, which has been previously observed [31,32]. In cell proliferation test (Fig. 3b), miRNA 24-3p have no cell proliferation effect, and no difference ($p > 0.05$) was observed between miRNA 24-3p and the negative control (miRNA NC, a disordered miRNA) group on days 2 and 4. Based on Fig. 3c–f, miRNA 24-3p could significantly promote cell migration and cell chemotaxis, and a significant difference was observed with miRNA NC ($p \leq 0.001$). Similarly, qRT-PCR test was used to verify the expression of migration-related genes (Fig. 3g). MiRNA NC had a false-positive expression in the expression of all migration-related genes compared with the control group. Notably, the expression of all migration-related genes in miRNA 24-3p group was significantly up-regulated compared with miRNA NC ($p \leq 0.05$). Based on the comprehensive analysis of the results of cell wound healing, cell chemotaxis and the expression of migration-related genes, miRNA 24-3p was a promising functional miRNA for promoting RCEC migration.

3.4. *In vivo corneal epithelial healing treated with Exos-miRNA 24-3p*

Exosomes can be used as an effective carrier for the synthetic miRNA 24-3p mimics/agomir. To solve the problem of the synthetic miRNA 24-3p mimics/agomir (e.g., difficulty in entering cells, easy degradation and short half-life), we used electroporation to transfer miRNA 24-3p mimics/agomir into the Exos to obtain Exos-miRNA 24-3p (Fig. S2). After the above preparations, the Exos-miRNA 24-3p was used for *in vivo* animal models of corneal epithelial defect to verify its effects (Fig. 4). The rabbit corneal epithelial defect models through physical trauma were successfully established and intervened with Exos-miRNA 24-3p by conjunctive injection (Fig. 4a). Reepithelialization was labeled with fluorescein sodium (Fig. 4c). According to wound healing in the first 3 days, wound trace was marked with different colours (Fig. 4d) and analysed quantitatively (Fig. 4b). On post-operative day 1, all groups had closure progress, but the control group (blank control group) had faster closure and was different from the PBS group (negative control group), Exos or Exos-miRNA NC ($p \leq 0.05$). Furthermore, the Exos-miRNA 24-3p group had fast closure, but no difference was observed with the control group ($p > 0.05$). On post-operative day 2, the wound healing rate of the PBS group was the slowest compared with the other groups ($p \leq 0.05$). The wound healing rate of the Exos-miRNA 24-3p group reached 94.26% and was the fastest in all groups. On post-operative day 3, only Exos-miRNA 24-3p group completed re-epithelization, while the other groups were not completely re-epithelised, and the re-epithelised cells were unhealthy and widely distributed in the diffusion. In PBS group, the remaining 2.3% were not re-epithelialized. The Exos, Exos-miRNA NC and Exos-miRNA 24-3p group showed a faster closing speed, especially the Exos-miRNA 24-3p group compared with the PBS group.

Corneal tissues were analysed by HE staining to observe the development of corneal epithelium (Fig. 4e and f). At 7 days after the injection of Exos-miRNA 24-3p under conjunctiva, the regenerated epithelial cells of the control and PBS group showed an irregular cell structure and obvious epithelial hypertrophy compared with native cornea. Especially in the PBS group, no mature basal columnar cells were observed. The Exos, Exos-miRNA NC and Exos-miRNA 24-3p group had epithelial structures similar to native cornea, with basal, wing and superficial cells. In comparison with the corneal epithelial thickness of native cornea (27.5 ± 3.83 μm), only the Exos-miRNA NC and Exos-miRNA 24-3p group had no difference ($p > 0.05$), but the thickness of Exos-miRNA 24-3p group was the closest (28.2 ± 3.45 μm, Fig. 4g). On post-operative day 12 (Fig. 4h), the control group had obvious recovery. Its epithelial hypertrophy disappeared, but the epithelium remained unhealthy and loose between cells. The epithelial cells in the PBS group were in the same state as those on day 7 without an epithelial cell structure and with cell hypertrophy. In the Exos, Exos-miRNA NC and Exos-miRNA 24-3p group, compared with the condition in day 7, the epithelial cell structure was clearer, and the cells were more mature and stable. Moreover, the number of layers and thickness of corneal epithelium in the Exos group, Exos-miRNA NC and Exos-miRNA 24-3p were the same as those in native cornea. In summary, the engineered exosomes, Exos-miRNA 24-3p, have more advantages in promoting corneal epithelial wound closure.

3.5. *Immunofluorescence and immunohistochemistry analysis after Exos-miRNA 24-3p treatment*

To further analyse the corneal epithelial defect models treated with Exos-miRNA 24-3p, we detected the expression of CK3 and ZO-1 proteins in RCECs by immunofluorescence (Fig. 5). On day 7, the control and experimental groups had lower expression of CK3 in corneal epithelium than the native cornea (Fig. 5a and b). However, the expression of CK3 in Exos-miRNA NC and Exos-miRNA 24-3p group was significantly up-regulated compared with the PBS or control group, and significant differences were observed ($p \leq 0.001$). Interestingly, CK3 was highly expressed in corneal stroma after physical trauma, which was the most obvious in PBS and control group. In all groups, the CK3 proteins that infiltrated into corneal stroma in Exos-miRNA 24-3p group were the least and the closest to native cornea. In addition, all groups expressed ZO-1 proteins, especially the Exos-miRNA 24-3p group, which formed an obvious tight junction (such as ZO-1) on the epithelial surface. Among all groups, the expression of ZO-1 proteins in Exos and Exos-miRNA NC group was higher than that in the PBS and control group ($p \leq 0.05$), but the Exos-miRNA 24-3p group was the closest to native cornea. On day 12, all groups progressed to varying degrees (Fig. 5c and d), and the area of CK3 proteins that infiltrated into corneal stroma remarkably decreased. CK3 proteins that infiltrated into corneal stroma in Exos-miRNA 24-3p group were the least and more similar to native cornea. CK3 proteins that infiltrated into corneal stroma in PBS, Exos, Exos-miRNA NC group and control group were highly expressed. In addition, the PBS and control group expressed the least CK3 protein in corneal epithelium, and significant differences were observed ($p \leq 0.001$). The Exos-miRNA 24-3p group had the highest expression of CK3, and no significant differences were observed between the Exos-miRNA 24-3p and native cornea group ($p > 0.05$). In the expression of ZO-1 proteins, expression was observed on the surface of corneal epithelial layer. The positive ZO-1 proteins of Exos and Exos-miRNA NC group were significantly higher than that of the PBS and control group ($p \leq 0.01$), in which Exos-miRNA 24-3p group was the highest and most similar to native cornea.

According to the qRT-PCR results of migration-related genes, the corresponding proteins were selected for further analysis. EGFR and MMP9 were labeled and analysed by immunohistochemistry (Fig. 5). In EGFR expression, PBS group had the least expression, followed by control group, Exos and Exos-miRNA NC group, and the expression of Exos-miRNA 24-3p group was the most similar to that of native cornea on day 7. Significant differences in the control, PBS, Exos and Exos-miRNA NC group were obtained with the native cornea group ($p \leq 0.05$). All groups had high expression of EGFR, and no differences were observed on day 12 ($p > 0.05$). In MMP9 expression, all groups expressed MMP9 and came close to the native cornea, and no significant differences were observed on days 7 and 12.

3.6. *Preparation and characterisation of thermosensitive hydrogel*

In the present work, we designed and developed a thermosensitive hydrogel for exosomes delivery. Firstly, we modified hyaluronic acid with methacrylic anhydride (HAMA). The double bond on HAMA was

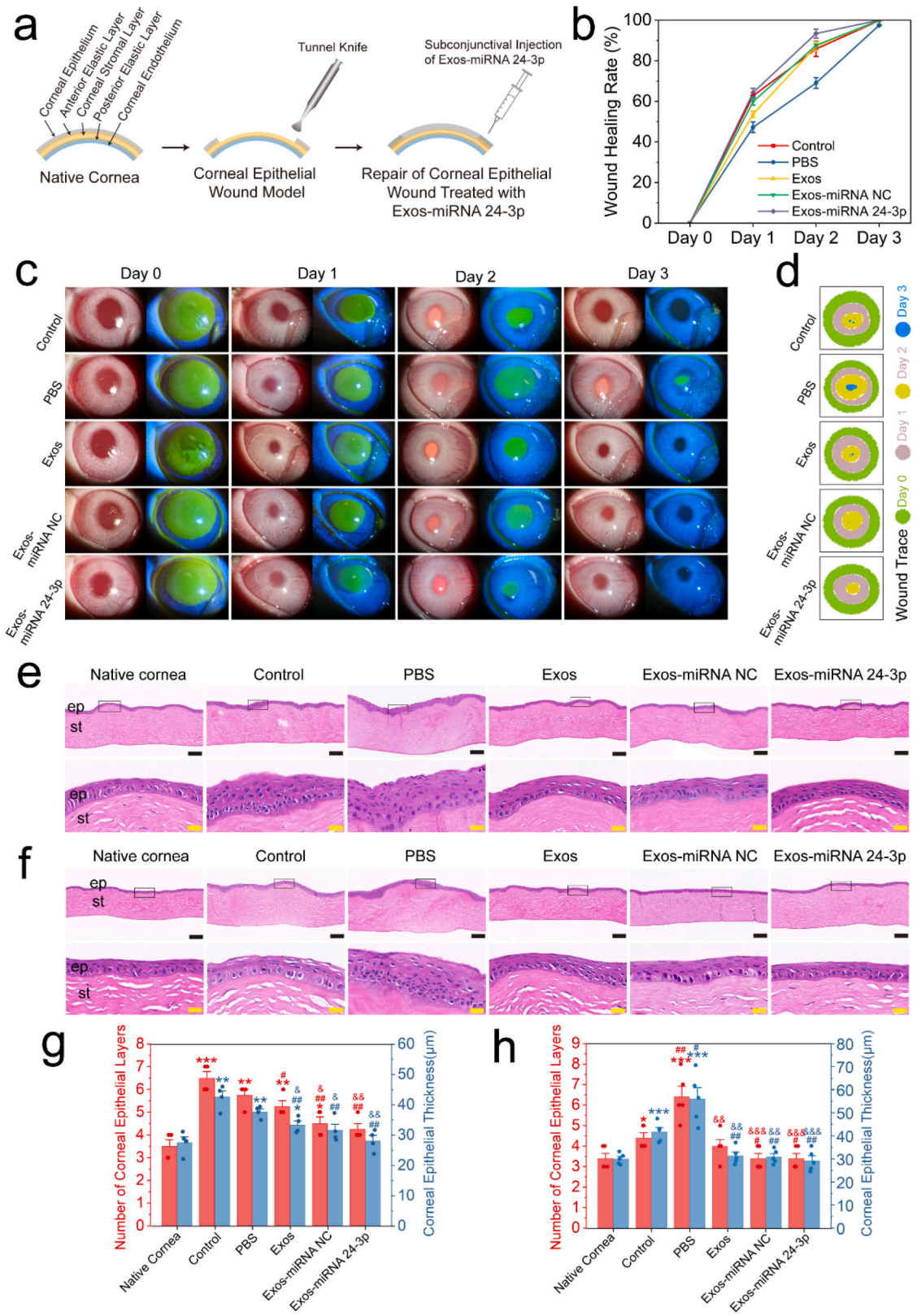

Fig. 4. *In vivo* animal experiment of Exos-miRNA 24-3p. (a) Establishment of animal model of corneal epithelial wound and the perioperative treatment. (e) Wound healing rate of corneal epithelium within 3 days. (c) Changes of corneal epithelial wound closures in rabbits within 3 days. Re-epithelialization of cornea was labeled with fluorescein sodium. (d) Traces of wound closures. HE staining of rabbit corneal tissue on days (e) 7 and (f) 12. ep: corneal epithelium, st: corneal stroma. Black scale bar: 100 μm; yellow scale bar: 20 μm. Rabbits corneal epithelial thickness and number of layers on day (g) 7 and (h) 12. The corneal thickness and layers of 4 different areas in Fig. 4g were used for statistical analysis; The corneal thickness and layers of 5 different areas in Fig. 4h were used for statistical analysis. ep: epithelium, st: stroma. *p ≤ 0.05, **p ≤ 0.01 and ***p ≤ 0.001 for native cornea; #p ≤ 0.05, ##p ≤ 0.01 and ###p ≤ 0.001 for control; &p ≤ 0.05, &&p ≤ 0.01 and &&&p ≤ 0.001 for PBS.

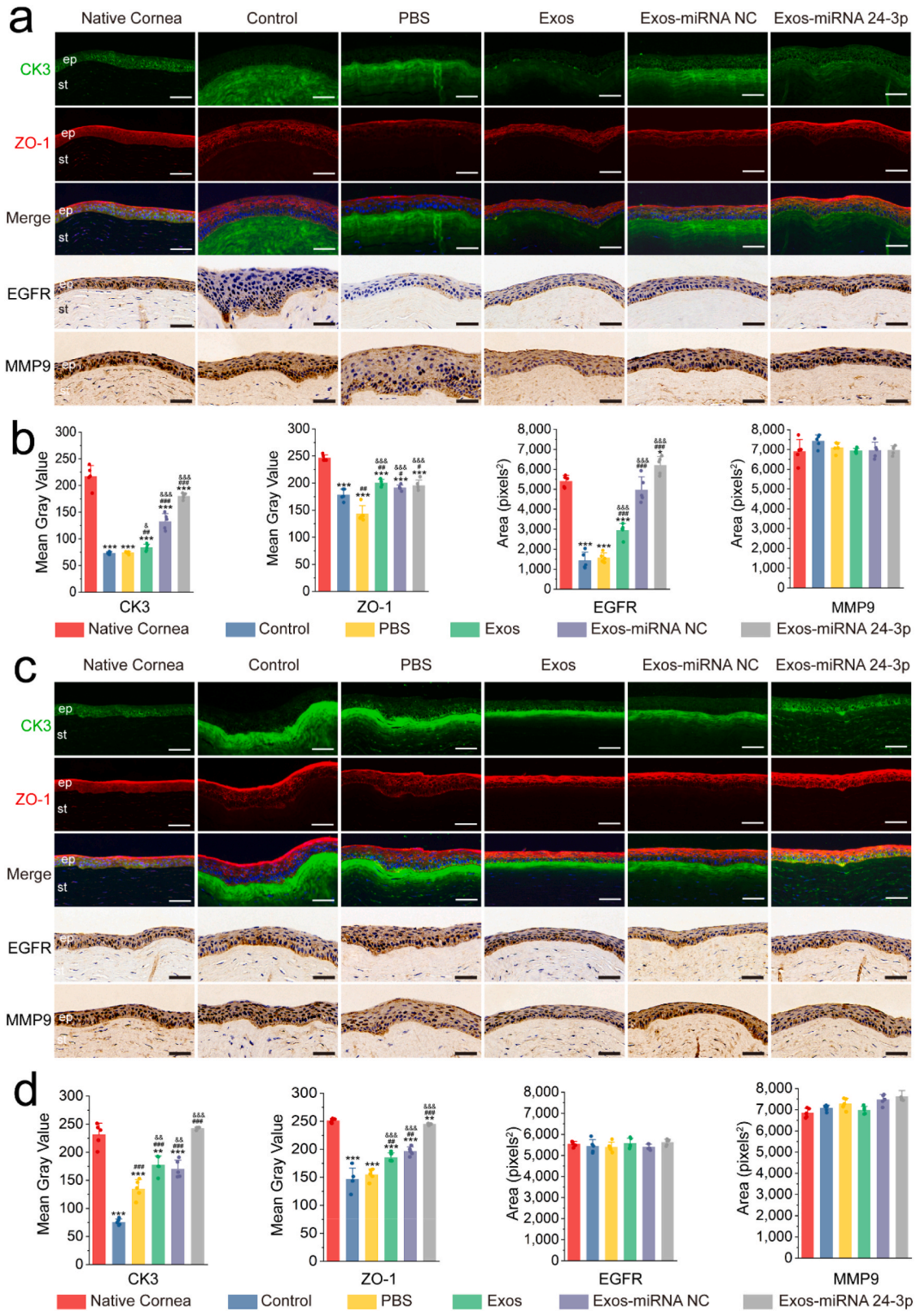

Fig. 5. Immunofluorescence and immunohistochemistry after Exos-miRNA 24-3p treatment. CK3, ZO-1, EGFR and MMP9 of the corneal epithelial defect models were treated with PBS, Exos, Exos-miRNA NC and Exos-miRNA 24-3p on (a and b) days 7 and (c and d) 12. Nuclei (blue) were labeled with DAPI in the merge image of c. Immunofluorescence or immunohistochemical semi-quantitative analysis on day 7 (b) or 12 (d) was performed using imageJ (n = 5). ep: epithelium, st: stroma. *p ≤ 0.05, **p ≤ 0.01 and ***p ≤ 0.001 for native cornea; #p ≤ 0.05, ##p ≤ 0.01 and ###p ≤ 0.001 for control; &p ≤ 0.05, &&p ≤ 0.01 and &&&p ≤ 0.001 for PBS. Scale bar: 50 μm.

then grafted with temperature-sensitive DEGMA to obtain thermosensitive DEGMA-modified hyaluronic acid (referred to as HD, Fig. 6a). The successful synthesis of HD was confirmed by ^{1}H NMR (Fig. 6b). The double bond characteristic peak a and b of HAMA appeared at 5.5–6.5 ppm, while the double bond characteristic peak of HD disappeared at this position, indicating that the double bond of HD was completely reacted. The synthetic HD had the characteristic peak d of DEGMA at 4.22 ppm, the terminal methyl characteristic peak f of DEGMA at 3–3.5 ppm, the characteristic peaks e of other methylene on the side chain between 3.5 and 4 ppm, and the hydrogen on DEGMA skeleton chain of approximately 1 ppm. These results provide sufficient evidence for the successful preparation of HD.

HD was dissolved in PBS or pure water with different concentrations (1, 3 and 5 wt%) when it formed thermosensitive DEGMA-modified hyaluronic acid hydrogel (THH) at 37 °C and named as THH-1, THH-3 and THH-5. THH-3 was dripped on the ocular surface of a rabbit and blinked instantly, then OCT was used for THH-3 imaging (Fig. 6c). THH-3 was distributed evenly on the ocular surface and had high transparency, implying that it can be used as a controlled release system for ocular surface without affecting visual lines. THH with different concentrations was also tested at 37 °C (Fig. 6d). All groups were in a sol state at 4 °C, and the sol to-gel transition could be achieved when the concentration was greater than 3 wt% at 37 °C. After injecting THH sol into PBS at 37 °C, THH was injectable, and the stability of THH was improved with the increase of HD concentration (Fig. 6e). The dissolution of THH-1 in PBS was mainly caused by its failure to form glue. The internal structure of THH with different concentrations was measured by SEM at 4 and 37 °C (Fig. 6f). The pore size decreased with increasing THH concentration. It had smaller pore and more networks at 37 °C than at 4 °C mainly because of the hydrophilic–hydrophobic interaction of DEGMA side chain. Interestingly, all groups showed a tubular structure, and no network connection was observed between the tubes at 4 °C. However, an obvious network was observed between tubes, and it increased with increasing THH concentration at 37 °C. The results were attributed to the principle of ice crystal formation. Moreover, the performance of THH was analysed by temperature, frequency and strain scanning by a rheometer (Fig. 6g). The results of temperature scanning showed that THH-1 could not be changed to gel with temperature ($G' < G''$); THH-3 could change from sol to gel at 37 °C ($G' = G''$), and THH-5 could change from sol to gel at 31 °C ($G' = G''$). The results of frequency scanning showed that under a constant temperature of 37 °C and strain of 1%, THH-1 and THH-3 undergo shear thinning when the angular frequency was greater than 10 rad/s, whereas THH-5 did not undergo shear thinning in the range of 0.1–100 rad/s. The results of strain scanning showed that under constant temperature of 37 °C and angular frequency of 10 rad/s, THH-1 was in the sol state, and THH-3 and THH-5 underwent shear thinning when the strain was greater than 316%. Ophthalmic hydrogels should have the ability to change sol-gel with temperature and shear thinning properties. To verify the biosafety of THH-3, we dripped THH-3 onto the ocular surface and observed it by HE and Masson staining (Fig. S3). THH-3 had excellent safety, and no inflammatory factors were produced. The same goblet cells were observed in the experimental group and normal conjunctival tissue. Therefore, THH-3 is an ideal ophthalmic hydrogel material.

3.7. Evaluation of THH-3/Exos-miRNA 24-3p treatment in alkali burn animal model

To improve the bioavailability of Exos-miRNA 24-3p and the safety of Exos-miRNA 24-3p delivery methods, we subjected Exos-miRNA 24-3p to controlled release by THH-3 in the ocular surface. Before the animal studies, the release method or model of Exos-miRNA 24-3p-FAM in THH-3 was shown in Fig. 7a. The Exos-miRNA 24-3p-FAM released from THH-3 passed through the Transwell into the RCECs in the lower chamber. The fluorescence expression of FAM labeled miRNA 24-3p mimics (miRNA 24-3p-FAM) and Exos-miRNA 24-3p-FAM released from THH-3 was observed through confocal microscopy in RCECs within 7 days (Fig. 7b). After co-incubation in day 1, the synthetic miRNA 24-3p-FAM was not expressed in RCECs. However, the fluorescence expression of Exos-miRNA 24-3p-FAM was found in RCECs. In addition, when the cells were observed on days 2, 4 and 7, the fluorescence of Exos-miRNA 24-3p-FAM was always expressed in the cells (Fig. S4).

In the present study, another animal model of corneal epithelial defect, namely, the alkali burn, was established, and the alkali burnt corneas *in vivo* were treated with THH3, Exos-miRNA 24-3p and THH-3/Exos-miRNA 24-3p (Fig. 7c). The treatment was administered as follows: once a day for the first 7 days, once every 3 days for 7–14 days and once per 7 days for 14–28 days (Fig. 7d). Corneal defects established by alkali burn were intervened with THH-3/Exos-miRNA 24-3p and observed with a slit lamp for 28 days (Fig. 7e and f). The macroscopic results showed the dynamic change process of alkali burn pathology. Firstly, the cornea became gradually transparent after epithelial healing in the first 7 days. Thereafter, the cornea gradually became turbid and formed edema, which was alleviated under the continuous intervention of THH-3/Exos-miRNA 24-3p. Fluorescein sodium staining (Fig. 7g) showed that the cornea epithelium could fall off under NaOH. THH-3/Exos-miRNA 24-3p treatment could substantially accelerate the healing of epithelial cells. Based on the calculation of the area of wound closure on day 1 (Fig. 7h), the cornea treated with THH-3/Exos-miRNA 24-3p could reach more than 85%, while that in PBS group was only 70%, and a significant difference was observed ($p \leq 0.001$). In comparison with the PBS group, Exos-miRNA 24-3p and THH-3/Exos-miRNA 24-3p group could accelerate corneal epithelial healing, especially THH-3/Exos-miRNA 24-3p, and a significant difference was observed ($p \leq 0.001$); for the THH-3 group, it had no effect on corneal epithelial healing. Overall, Exos-miRNA 24-3p has an excellent effect on accelerating corneal epithelial healing, but the use of THH-3 as a controlled release system of Exos-miRNA 24-3p is more effective.

3.8. Post-operative observation by In vivo confocal microscopy, OCT and HE staining

In vivo confocal microscopy was used to observe the transparent corneal tissue after repair, including corneal epithelium, corneal stroma and corneal endothelium (Fig. 8a). All groups had normal corneal epithelium and endothelial cells after repair, but the corneal stroma treated with PBS was turbid. OCT was used to observe the internal changes of cornea after treatment with THH-3/Exos-miRNA 24-3p (Fig. 8a). In comparison with native cornea (405 μm), the corneal thickness increased significantly in the PBS group (1045 μm), THH-3 (875 μm), Exos-miRNA 24-3p (791 μm) and THH-3/Exos-miRNA 24-3p (765 μm) mainly because of corneal edema and fibrosis. In terms of the scope of post-operative corneal edema, the alkali burnt cornea treated with THH-3/Exos-miRNA 24-3p (3826 μm) was significantly smaller than that in the PBS group (4524 μm). Overall, both THH-3 and Exos-miRNA 24-3p can inhibit further corneal edema, no synergistic effect was observed between them.

To further observe the alkali burned corneal tissues after THH-3/Exos-miRNA 24-3p treatment, we used HE staining to analyse the internal structure of cornea (Fig. 8b) and carried out quantitative analysis (Fig. 8c and d). On day 7, both Exos-miRNA 24-3p and THH-3/Exos-miRNA 24-3p group had healthy and complete epithelial layer, and no difference was observed in the thickness and number of layers ($p > 0.05$). The PBS and THH-3 group had thinner epithelial layer, significant differences were observed in the thickness and number of layers compared with native cornea ($p \leq 0.05$). Except for PBS group and THH-3, the thickness and number of layers of epithelium in Exos-miRNA 24-3p and THH-3/Exos-miRNA 24-3p group increased significantly and were similar to those of the epithelium of native cornea. In addition to epithelial differences, corneal stroma also differed. The corneal stroma was irregular and had many large cavities caused by tissue edema, and the fibroblasts/corneal stromal cells were activated in PBS group and

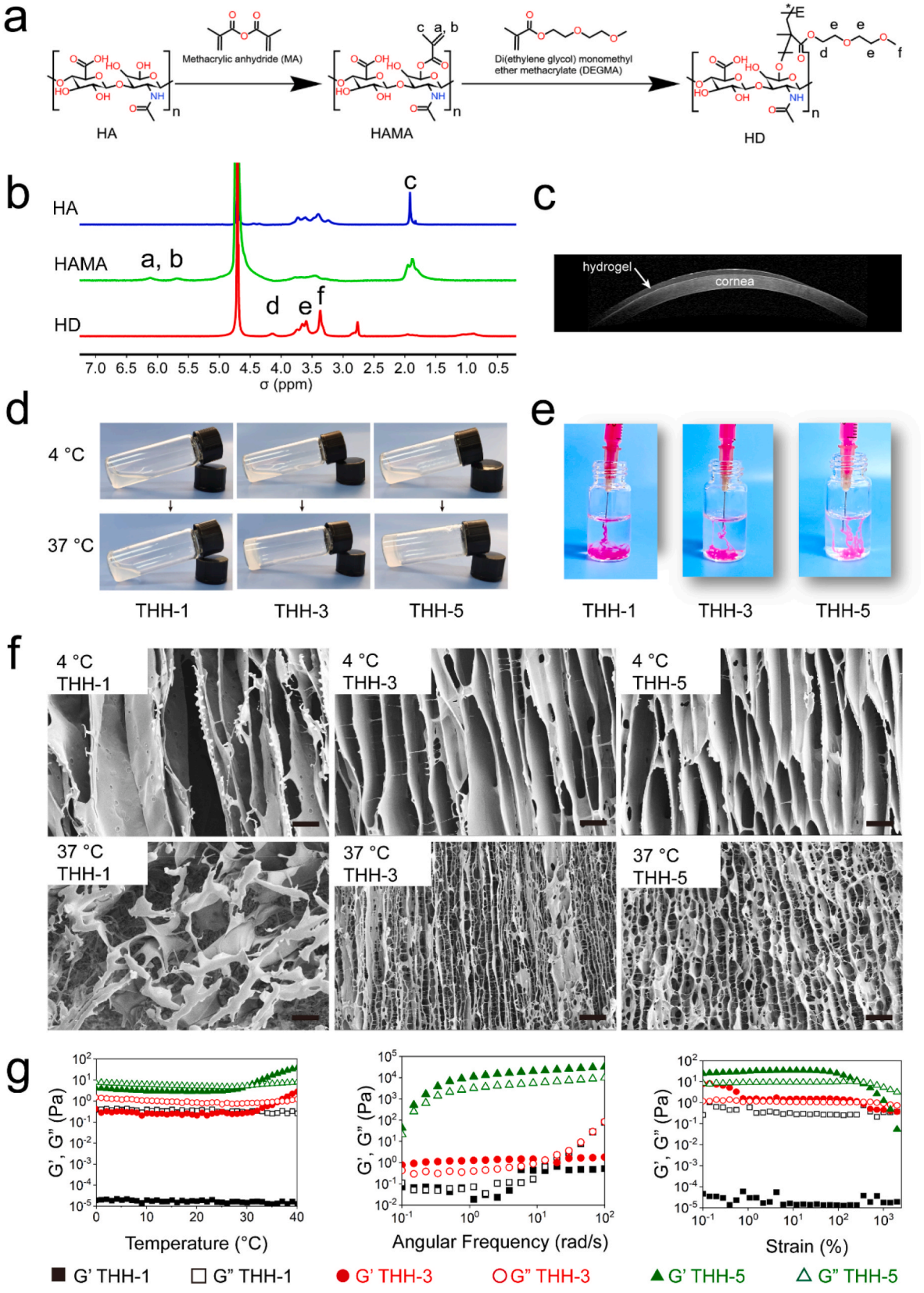

Fig. 6. Preparation and characterisation of HD and THH. (a) Synthetic route of HD. (b) ^{1}H NMR of HA, HAMA and HD. (c) Stability and gelation properties of THH-3 on rabbit eye. (d) Sol-gel transition of THH-1, THH-3 and THH-5 from 4 to 37 °C. (e) Stability of THH-1, THH-3 and THH-5 in PBS at 37 °C. (f) SEM of THH-1, THH-3 and THH-5 at 4 and 37 °C. Scale bar: 20 μm. (g) Temperature scanning, frequency scanning and strain scanning of THH-1, THH-3 and THH-5 as determined using a rheometer.

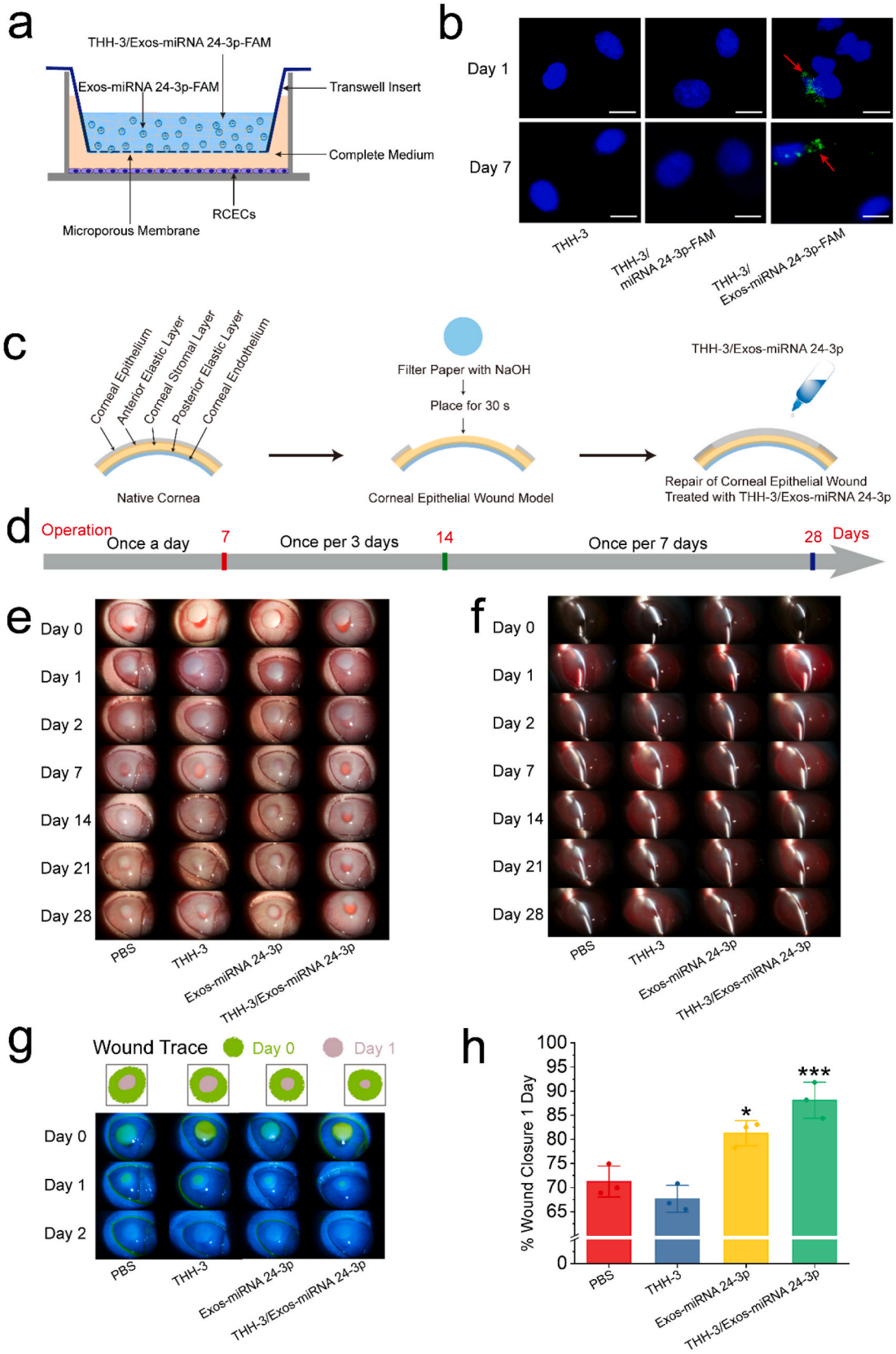

Fig. 7. *In vitro* release of Exos-miRNA 24-3p in THH-3 and *in vivo* evaluation of THH-3/Exos-miRNA 24-3p in a rabbit corneal epithelial defect model of alkali burn. (a) The release diagram of Exo-miRNA 24-3p in THH-3. (b) The release of Exo-miRNA 24-3p in THH-3 on days 1 and 7. The red arrows indicated the FAM-labeled miRNA 24-3p in Exos. Scale bar: 20 μm. (c) Establishment of animal model of corneal alkali burn and the perioperative treatment. (d) Prescription for eye medication. (e and f) Slit lamp photographs days 0, 1, 2, 7, 14, 21 and 28 after operation. (g) Wound trace and fluorescein sodium staining 0, 1 and 2 days after operation. (h) Wound closure rate 1 day after operation. *$p \leq 0.05$, **$p \leq 0.01$ and ***$p \leq 0.001$ for PBS.

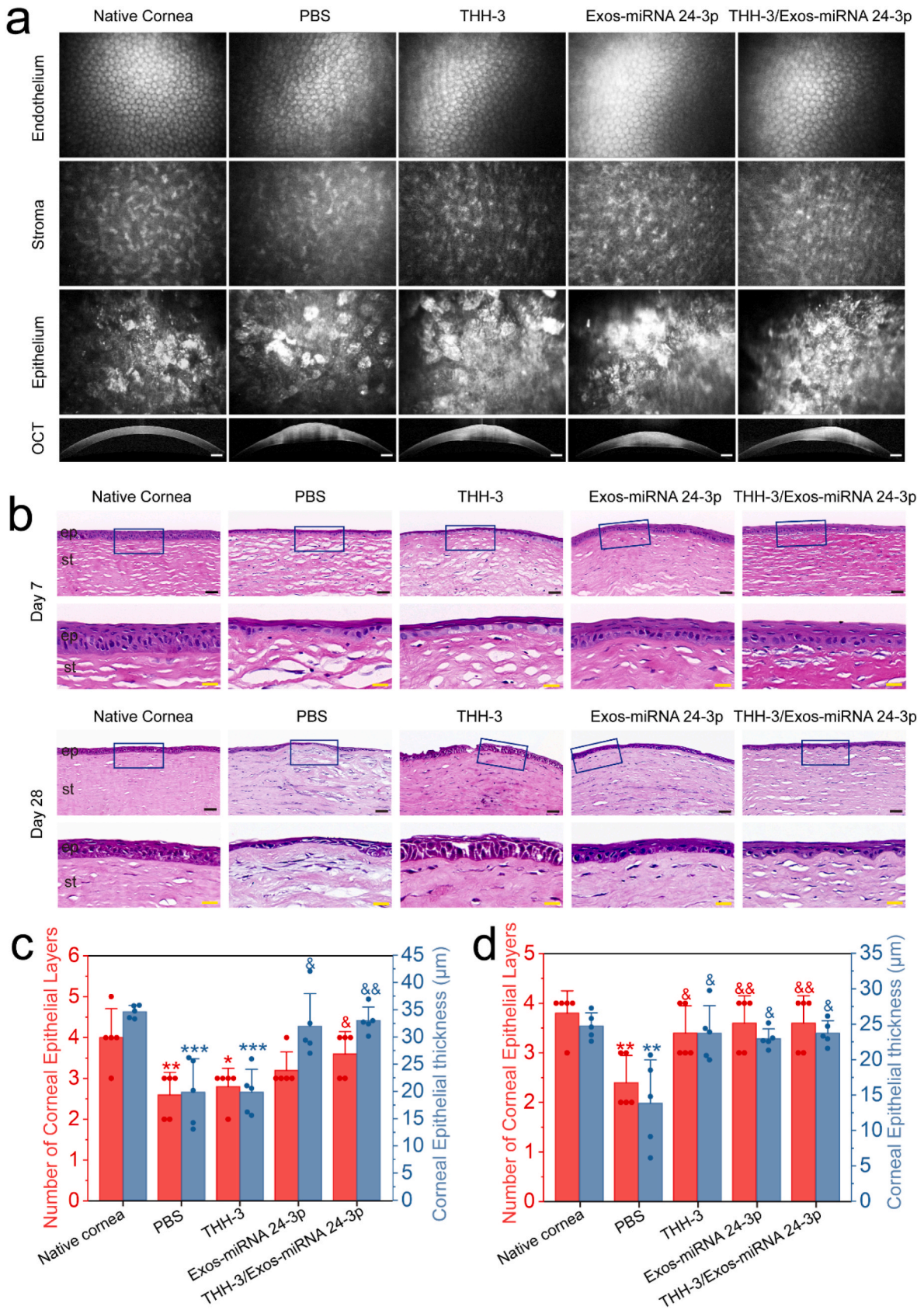

Fig. 8. *In vivo* evaluation of THH-3/Exos-miRNA 24-3p in a rabbit corneal epithelial defect model of alkali burn. (a) Anterior segment optical coherence tomography (OCT) images and *in vivo* confocal microscopy of rabbit corneas after 28 days of alkali burn treatment. Scale bar of the OCT images: 500 μm. (b) HE staining of rabbit corneal tissues on days 7 and 28. ep: epithelium, st: stroma. Black scale bar: 50 μm; yellow scale bar: 20 μm. Rabbit corneal epithelial thickness and number of layers of corneal epithelial on days (c) 7 and (d) 28 (n = 5). *p ≤ 0.05, **p ≤ 0.01 and ***p ≤ 0.001 for native cornea; &p ≤ 0.05, &&p ≤ 0.01, &&&p ≤ 0.001 for PBS.

THH-3. This phenomenon prompted the differentiated corneal stromal cells to secrete type I collagen, resulting in corneal scar formation. On day 28, the cornea treated with Exos-miRNA 24-3p and THH-3/Exos-miRNA 24-3p continued to maintain healthy epithelial tissue, and the thickness and number of layers of epithelium were similar to those of native cornea. The PBS group also maintained a pathological corneal epithelium with only two layers of cells and spherical basal cells. Interestingly, the cornea treated with THH-3 recovered the normal corneal thickness, but the morphology of corneal epithelial cells was poor, and the cells had no tight junction. In comparison with native cornea, Exos-miRNA 24-3p group had healthy corneal epithelium, but the thickness was different ($p \leq 0.05$). Differences were observed among THH-3, Exos-miRNA 24-3p and THH-3/Exos-miRNA 24-3p group compared with the PBS group ($p \leq 0.05$). Edema was caused by inflammation in the corneal stroma of PBS group.

3.9. Immunofluorescence analysis after THH-3/Exos-miRNA 24-3p treatment

To confirm whether cornea tissue has been successfully repaired, we used immunofluorescence of CK3 and ZO-1 proteins to evaluate the molecular level of corneal epithelial repair (Fig. 9). All groups completed corneal re-epithelization and had different degrees of CK3 and ZO-1 expression in corneal epithelial tissue at 7 days after operation (Fig. 9a and b). The PBS and THH-3 group showed low expression of CK3. In all groups, no difference in CK3 expression was observed between THH-3/Exos-miRNA 24-3p group and natural cornea ($p > 0.05$). ZO-1 had a low expression in the PBS, THH-3 and Exos-miRNA 24-3p group, and significant differences were observed with native cornea ($p \leq 0.001$). Zo-1 expression was higher in the THH-3/Exos-miRNA 24-3p group compared with PBS group ($p \leq 0.001$), showing an excellent corneal epithelial repair effect of THH-3/Exos-miRNA 24-3p in the first 7 days. On day 28 after the operation (Fig. 9c and d), the PBS and THH-3 group still had low expression of CK3, and significant differences were observed with native cornea ($p \leq 0.001$), indicating that corneal epithelial cells are immature. ZO-1 was highly expressed in all groups except PBS group and similar to native cornea ($p > 0.05$).

EGFR and MMP9 could regulate the migration of corneal epithelial cells, resulting in corneal epithelial wound healing. Accordingly, EGFR and MMP9 in corneal epithelium were detected by immunofluorescence (Fig. 9). On day 7 after the operation (Fig. 9a and b), EGFR and MMP9 were not expressed in the PBS group. The THH-3 group expressed MMP9 but not EGFR, and MMP9 expression was low in the THH-3, Exos-miRNA 24-3p and THH-3/Exos-miRNA 24-3p group. Importantly, EGFR expression was higher in the Exos-miRNA 24-3p and THH-3/Exos-miRNA 24-3p group compared with the PBS and THH-3 group ($p \leq 0.001$), which was similar to that in native cornea group. On day 28 after the operation (Fig. 9c and d), only PBS group had low expression of EGFR, while other groups had high expression of EGFR and MMP9, but they had significant differences with native cornea ($p \leq 0.05$). Interestingly, within 28 days after alkali burn, the corneal stroma had low MMP9 expression, indicating alkali burn can continuously produce inflammation to the corneal stroma. By contrast, the PBS group had high expression of MMP9, while the THH-3/Exos-miRNA 24-3p group had the lowest expression. Therefore, THH-3/Exos-miRNA 24-3p can inhibit the further production of inflammation.

α-SMA can be used to identify corneal fibrosis, and CD163 can be used to label M2 macrophages. On day 7 after the operation (Fig. 9a and b), α-SMA and CD163 were highly expressed in the PBS group, followed by the THH-3 and Exos-miRNA 24-3p group but the lowest in the THH-3/Exos-miRNA 24-3p group. The α-SMA and positive CD163 expression of Exos-miRNA 24-3p and THH-3/Exos-miRNA 24-3p group was significantly different from that of the PBS group ($p \leq 0.001$). On day 28 after the operation (Fig. 9c and d), α-SMA expression was higher in the PBS, THH-3 and Exos-miRNA 24-3p compared with native cornea ($p \leq 0.001$) but not in the THH-3/Exos-miRNA 24-3p group ($p > 0.05$), indicating that THH-3/Exos-miRNA 24-3p can inhibit corneal fibrosis. CD163 expression was downregulated compared with condition 7 days after operation, but low M2 macrophage expression was still observed in all groups, suggesting that all corneas are in the repair stage, and the inflammation is relieved.

4. Discussion

A series of pathological problems after corneal epithelial defect can be addressed by accelerating the healing of corneal epithelium. The healing of corneal epithelial is a complex and coordinated physiological process, and it involves cell migration, proliferation, adhesion and differentiation with cell layer stratification [33]. The growth factor/cytokine and extracellular matrix signal-mediated interactions at the wound site can re-establish epithelial integrity and restore corneal homeostasis [34]. Several techniques and materials are currently available for treatment of corneal epithelial defect, and many of these methods involve complex procedures and use techniques or materials with poor biocompatibility, safety and effectiveness. Ideally, any newly developed techniques and materials should be easily applied in a clinical setting, readily corneal epithelial healing, even corneal stromal repair. Moreover, these methods should reduce the frequency of eye medication and have the effect of continuous administration.

In previous studies, some researchers used corneal mesenchymal stromal cell or mesenchymal stem cells derived from human bone marrow or exosomes derived from corneal epithelial cell for the treatment of corneal wound healing [35–37], showing ideal repair effect, but the mechanism in which exosomes participate in corneal wound healing remains still unclear. Among the various MSC sources, bone-derived MSCs (BMSCs) and ADSCs are the two most commonly used in preclinical and clinical tissue regeneration applications. While, umbilical cord-derived MSCs have also been widely employed in research and clinical trials. Their use in many applications is limited since they are not practical for autologous administration in adults. ADSCs are an attractive alternative as they are higher in frequency, more easily obtained and cause less donor site morbidity [38]. Furthermore, ADSCs display a higher proliferation rate than BMSCs *in vitro* and show a greater ability to maintain their stem cell characteristics, including self-renewal, proliferation, and differentiation potential, after repeated passaging [39]. Thus, we choose ADSCs as our material source. Scholars agree that the role of stem cells is achieved via its paracrine. In addition to endowing the same functions as ADSCs, Exos are an outstanding transport carrier, which can enter target cells by endocytosis.

MiRNA 24-3p, which belongs to the miRNA 24 family, plays a significant role in cancer initiation and progression [40]. The majority of cancer cells are epithelial in origin, beginning in a tissue that lines the inner or outer surfaces of the body. Thus, we hypothesized that miRNA 24-3p has the same migration effect on corneal epithelial cells. In the cell migration experiment, miRNA 24-3p mimics showed excellent effects in cell chemotaxis, cell wound healing and the expression of migration-related genes, which might be due to the similarity of source between cancer cells and epithelioid cells. However, miRNA 24-3p acts in different pathways, so it does not mean that miRNA 24-3p can regulate all epithelioid cells. FGF signalling, which is involved in the control of cell proliferation, differentiation, migration, survival and polarity, is transduced through FGF receptors (FGFR) [41]. A key component of FGF signalling is the docking protein called FGFR substrate 2 (FRS2) which undergoes phosphorylation on tyrosine residues upon FGF stimulation [42,43]. CDC42, which is also known as cell division cycle protein, is a GTP-binding protein belonging to the Rho family of small GTPases. The expression of CDC42 has been linked to eye development and photoreceptor morphogenesis [44,45]. CDC42 is an important regulator of corneal epithelial wound repair [46]. CDC42 may interact with receptor tyrosine kinase-activated signalling cascades that participate in cell migration and cell-cycle progression [47]. CTGF is expressed in the native cornea, lens, iris and retina and is expressed

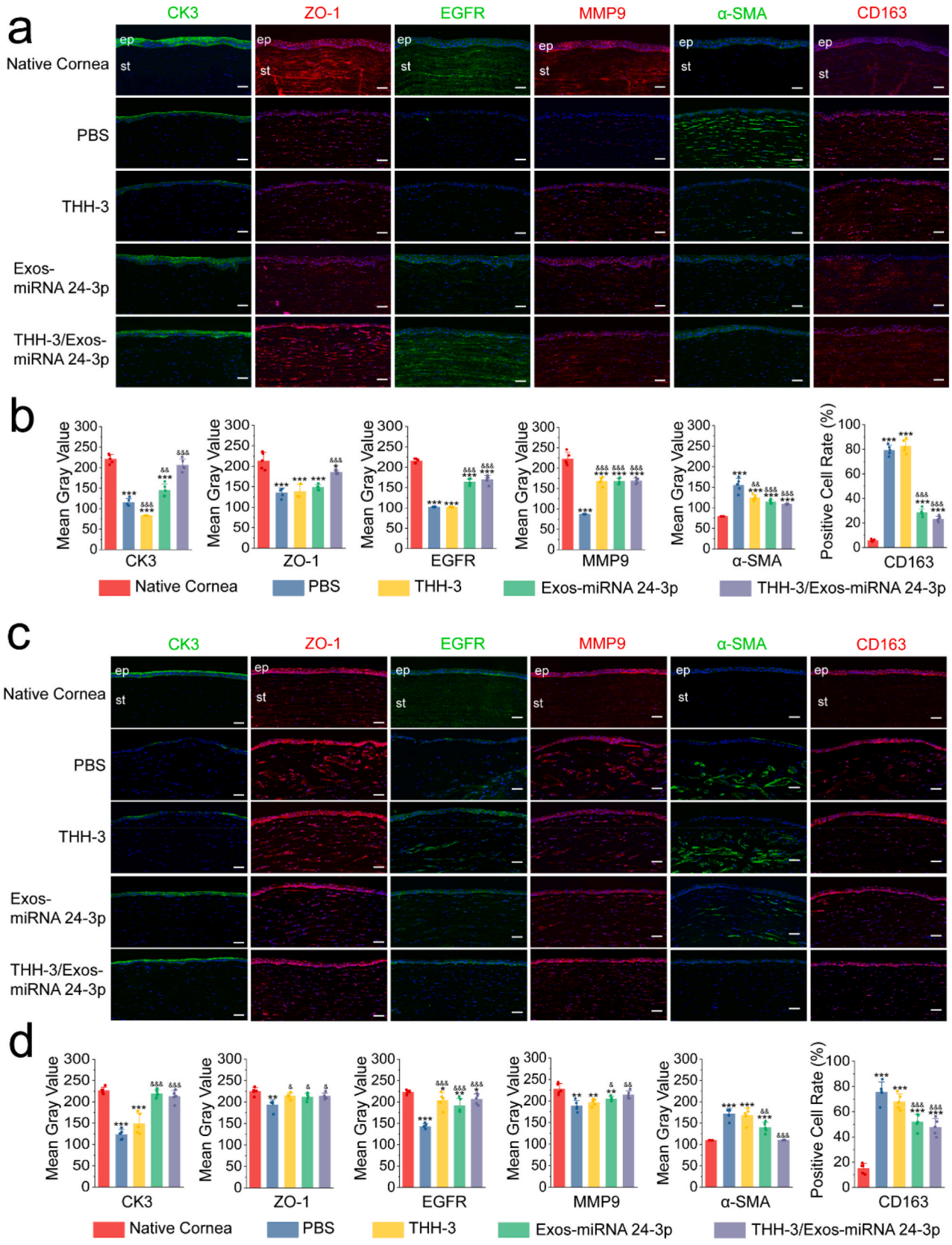

Fig. 9. CK3, ZO-1, EGFR, MMP9, α-SMA and CD163 of rabbit corneal tissues treated with THH-3/Exos-miRNA 24-3p on days (a) 7 and (b) 28. Immunofluorescence or immunohistochemical semi-quantitative analysis on day 7 (b) or 12 (d) was performed using imageJ. (n = 5). ep: epithelium; st: stroma. *p ≤ 0.05, **p ≤ 0.01 and ***p ≤ 0.001 for native cornea; #p ≤ 0.05, ##p ≤ 0.01 and ###p ≤ 0.001 for control; &p ≤ 0.05, &&p ≤ 0.01 and &&&p ≤ 0.001 for PBS. Nuclei (blue) were labeled with DAPI. Scale bar: 50 μm.

immediately after epithelial injury [48,49]. CTGF loss impairs efficient re-epithelialization of corneal wounds [50]. In the present study, miRNA 24-3p promoted the up-regulation of FRS2, CDC42, CTGF, EGFR and MMP9, mainly because miRNA 24-3p regulated the phosphorylation of tyrosine residues and the signal cascade activated by receptor tyrosine kinase in cell cycle process. Exos with low or no expression of miRNA 24-3p meet the conditions for loading miRNA 24-3p. Thus, we engineered the Exos via miRNA 24-3p to capacitate it an excellent migration ability for corneal epithelial healing. We successfully constructed a rabbit corneal epithelial defect model and treated it with Exos-miRNA 24-3p by subconjunctival administration. The results also confirmed the excellent migration ability of Exos-miRNA 24-3p. After trauma, the surrounding cells will secrete many factors and recruited granulocytes or macrophages for tissue repair [51,52]. Trauma may cause damage to the basement membrane and anterior elastic layer, allowing the secreted factors to easily enter the corneal stroma, which contains a large amount of keratin, including CK3. The expression of CK3 in corneal stroma will affect the corneal microenvironment. Exos-miRNA 24-3p could accelerate corneal epithelial wound healing, so only a small amount of CK3 entered the corneal stroma. Considering the limitation of antibody, we only selected EGFR and MMP9 for *in vivo* analysis. EGFR signalling is critical during embryogenesis, particularly in epithelial development, and the disruption of EGFR gene results in epithelial immaturity and perinatal death [53]. EGFR signalling also functions during wound-healing responses by accelerating wound re-epithelialization, thus inducing cell migration, proliferation and angiogenesis [54]. Interestingly, positive EGFR proteins were significantly less in untreated and PBS injected under conjunctiva on day 7 after operation. Therefore, the regenerated corneal epithelial cells in both groups were immature epithelial cells. The activated MMP9 regulated corneal epithelial cell migration by cleaving the ectodomain of β4 integrin between corneal epithelial cells and basement membrane [55]. In the expression of MMP9, no differences were observed among all groups, because MMP9 was mainly involved in epithelial migration during wound healing.

Subconjunctival administration must be carried out under local anaesthesia, resulting in brings risks to the treatment of corneal diseases [56]. It not only has high technical requirements for doctors, but also may damage the conjunctiva [57]. On topical application, the hydrogel, an ideal drug delivery system, may form a highly uniform and clear thin layer that conforms to the ocular surface and resists clearance from blinking, thus increasing the intraocular absorption of hydrophilic and hydrophobic drugs and extending the drug–ocular–epithelium contact time [25]. We modified sodium hyaluronate for eyes to induce it thermal sensitivity and thus form a highly uniform and clear thin layer on the ocular surface under body temperature. THH-3 was injectable, stable, and easy to operate. Most importantly, THH-3, as a controlled release system, can solve the problems of the instability and short retention time of Exos in ocular surface and improve the utilization efficiency of miRNA 24-3p.

Chemical alkali burn is one of the most common ophthalmic emergencies. It is a serious ocular trauma with long course, difficult vision recovery and severe sequelae [57]. It is difficult to treat with a single drug. In the present study, the THH-3 was used to control the slow release of Exos-miRNA 24-3p, achieving a better healing effect. Under low-to-no expression EGFR or MMP9, corneal epithelial migration will be affected, resulting in corneal epithelial abscission or lesions. Based on the experimental results, the expression of EGFR and MMP9 in corneal alkali burn diseases treated with THH-3/Exos-miRNA 24-3p remained similar to that in native cornea from day 7 to day 28. THH-3/Exos-miRNA 24-3p maintained the steady-state environment of corneal epithelial cell renewal. Therefore, the adaptive hydrogel, as a controlled release system, is very important for tissue repair.

5. Conclusion

In conclusion, we explored the optimal concentration of exosomes derived from ADSCs with biological function. There exosomes could promote the proliferation and migration of RCECs, regulate the vinculin expression and the up-regulation of migration-related genes. Subsequently, we hypothesized that miRNA 24-3p could regulate corneal epithelial cell migration, and fully verified its accelerating cell migration ability *in vivo* and *in vitro*. The ocular bioavailability and convenience of Exos-miRNA 24-3p were increased via developing a controlled release system with biocompatibility, stability and temperature sensitivity to slow release Exos-miRNA 24-3p. THH-3/Exos-miRNA 24-3p effectively promoted the migration and maturation of RCECs and regulated corneal microenvironment, including fibrosis inhibition and inflammatory reaction reduction. These processes remarkably enhanced the repair of alkali-burnt corneal tissue *in vivo*. This study provided a promising miRNA-based delivery strategy for the efficient and adaptative treatment of patients suffering from corneal alkali burn and an important theoretical basis for the development of cell-free therapy. Most importantly, this method follows the 'from nature to nature' principle.

Ethics approval and consent to participate

All animal experiments of the present study were performed according to the ARVO Statement for the Use of Animals in Ophthalmic and a protocol approved by the Animal Care Committee of South China University of Technology (AEC No. CV2020007), Guangzhou, China. All the authors listed have approved the animal study.

Notes

The authors declare no competing financial interest.

CRediT authorship contribution statement

Xiaomin Sun: conception and design, conduction of experiments, collection and/or assembly of data, data analysis and interpretation, manuscript writing. **Wenjing Song:** conduction of experiments, data analysis and interpretation, manuscript revision, final approval of manuscript. **Lijing Teng:** design and preparation of thermosensitive DEGMA-modified hyaluronic acid hydrogels. **Yongrui Huang:** data analysis and interpretation. **Jia Liu:** data analysis and interpretation. **Yuehai Peng:** conduction of experiments. **Xiaoting Lu:** conduction of experiments. **Jin Yuan:** conduction of experiments. **Xuan Zhao:** conduction of experiments. **Qi Zhao:** conduction of experiments. **Yingni Xu:** conduction of experiments. **Jingjie Shen:** drug purchase and expense reimbursement. **Xiaoyun Peng:** conduction of experiments. **Li Ren:** conception and design, data analysis and interpretation, manuscript revision, and final approval of manuscript.

Acknowledgments

This work was supported by the National Natural Science Foundation of China (32071333, 52173123), the Guangdong Province Key Field R&D Program Projects (2020B1111150002, 2019B010941002), the Guangdong Scientific and Technological Project (2021A1515010878), the Frontier Research Program of Bioland Laboratory (Guangzhou Regenerative Medicine and Health Guangdong Laboratory, 2018GZR110105008), the Science and Technology Planning Project of Guangzhou (202206010160) and the Fundamental Research Funds for the Central Universities.

Appendix A. Supplementary data

Supplementary data to this article can be found online at https://doi.org/10.1016/j.bioactmat.2022.07.011.

References

[1] S. Shukla, S.K. Mittal, W. Foulsham, E. Elbasiony, D. Singhania, S.K. Sahu, S. K. Chauhan, Therapeutic efficacy of different routes of mesenchymal stem cell administration in corneal injury, Ocul. Surf. 17 (2019) 729–736.

[2] S.R. Flaxman, R.R. Bourne, S. Resnikoff, P. Ackland, T. Braithwaite, M.V. Cicinelli, A. Das, J.B. Jonas, J. Keeffe, J.H. Kempen, Global causes of blindness and distance vision impairment 1990–2020: a systematic review and meta-analysis, Lancet Global Health 5 (12) (2017) e1221–e1234.

[3] A.A. Torricelli, S.E. Wilson, Cellular and extracellular matrix modulation of corneal stromal opacity, Exp. Eye Res. 129 (2014) 151–160.

[4] L. Lassance, G.K. Marino, C.S. Medeiros, S. Thangavadivel, S.E. Wilson, Fibrocyte migration, differentiation and apoptosis during the corneal wound healing response to injury, Exp. Eye Res. 170 (2018) 177–187.

[5] C.P. Lin, M. Boehnke, Effect of fortified antibiotic solutions on corneal epithelial wound healing, Cornea 19 (2000) 204–206.

[6] B. Wirostko, M. Rafii, D.A. Sullivan, J. Morelli, J. Ding, Novel therapy to treat corneal epithelial defects: a hypothesis with growth hormone, Ocul. Surf. 13 (2015) 204–212.

[7] M. Khan, K. Manuel, B. Vegas, S. Yadav, R. Hemmati, Z. Al-Mohtaseb, Case series: extended wear of rigid gas permeable scleral contact lenses for the treatment of persistent corneal epithelial defects, Contact Lens Anterior Eye 42 (2019) 117–122.

[8] M.A. Chappelet, D. Bernheim, C. Chiquet, F. Aptel, Effect of a new matrix therapy agent in persistent epithelial defects after bacterial keratitis treated with topical fortified antibiotics, Cornea 36 (2017) 1061–1068.

[9] H.S. Dua, A. Azuara-Blanco, Corneal allograft rejection: risk factors, diagnosis, prevention, and treatment, Curr. Ophthalmol. 47 (1999) 3–9.

[10] P. Furrer, J.M. Mayer, R. Gurny, Ocular tolerance of preservatives and alternatives, Eur. J. Pharm. Biopharm. 53 (2002) 263–280.

[11] G. Kafa, M. Horani, F. Musa, A. Al-Husban, M. Hegab, N. Asir, Marginal corneal infiltration following treatment for metastatic breast cancer with triple chemotherapy of Trastuzumab, Pertuzumab & Docetaxel, Ocul. Immunol. Inflamm. (2022) 1–6.

[12] T.C. Tapias, A.D. Díaz, R. Secondi, H.C. Villamil, J.S. España, Resolution of conjunctival melanoma with topical interferon alpha 2b in a patient with mitomycin C intolerance, Arch. Soc. Esp. Oftalmol. 93 (2018) 558–561.

[13] D.K. Jeppesen, A.M. Fenix, J.L. Franklin, J.N. Higginbotham, Q. Zhang, L. J. Zimmerman, D.C. Liebler, J. Ping, Q. Liu, R. Evans, Reassessment of exosome composition, Cell 177 (2019) 428–445.

[14] W. Liao, Y. Du, C.H. Zhang, F.W. Pan, Y. Yao, T. Zhang, Q. Peng, Exosomes: the next generation of endogenous nanomaterials for advanced drug delivery and therapy, Acta Biomater. 86 (2019) 1–14.

[15] N. Liu, X. Zhang, Li, M. Zhou, T. Zhang, S. Li, X. Cai, P. Ji, Y. Lin, Tetrahedral framework nucleic acids promote corneal epithelial wound healing in vitro and in vivo, Small 15 (2019), 1901907.

[16] Li, J.; Yao, Y.; Wang, Y.; Xu, J.; Zhao, D.; Liu, M.; Shi, S.; Lin, Y. Modulation of the crosstalk between schwann cells and macrophages for nerve regeneration: a therapeutic strategy based on multifunctional tetrahedral framework nucleic acids system. Adv. Mater. 2022, 2202513.

[17] Zhang, T.; Tian, T.; Lin, Y. Functionalizing framework nucleic acid-based nanostructures for biomedical application. Adv. Mater. 2021, 2107820.

[18] G.N. Alzhrani, S.T. Alanazi, S.Y. Alsharif, A.M. Albalawi, A.A. Alsharif, M.S. Abdel-Maksoud, N. Elsherbiny, Exosomes: isolation, characterization, and biomedical applications, Cell Biol. Int. 45 (2021) 1807–1831.

[19] A. Li, Y. Zhao, Y. Li, L. Jiang, Y. Gu, J. Liu, Cell-derived biomimetic nanocarriers for targeted cancer therapy: cell membranes and extracellular vesicles, Drug Deliv. 28 (2021) 1237–1255.

[20] J.P. Nederveen, G. Warnier, A. Di Carlo, M.I. Nilsson, M.A. Tarnopolsky, Extracellular vesicles and exosomes: insights from exercise science, Front. Physiol. 11 (2021), 604274.

[21] C. Ryall, S. Duarah, S. Chen, H. Yu, J. Wen, Advancements in skin delivery of natural bioactive products for wound management: a brief review of two decades, Pharmaceuticals 14 (2022) 1072.

[22] A. Verma, A. Tiwari, S. Saraf, P.K. Panda, A. Jain, S.K. Jain, Emerging potential of niosomes in ocular delivery, Expet Opin. Drug Deliv. 18 (2021) 55–71.

[23] C.H. Tsai, P.Y. Wang, I.C. Lin, H. Huang, G.S. Liu, C.L. Tseng, Ocular drug delivery: role of degradable polymeric nanocarriers for ophthalmic application, Int. J. Mol. Sci. 19 (2018) 2830.

[24] M. Mofidfar, B. Abdi, S. Ahadian, E. Mostafavi, T.A. Desai, F. Abbasi, Y. Sun, E. E. Manche, C.N. Ta, C.W. Flowers, Drug delivery to the anterior segment of the eye: a review of current and future treatment strategies, Int. J. Pharm. 607 (2021), 120924.

[25] Y.C. Kim, M.D. Shin, S.F. Hackett, H.T. Hsueh, E.S.R. Lima, A. Date, H. Han, B. J. Kim, A. Xiao, Y. Kim, Gelling hypotonic polymer solution for extended topical drug delivery to the eye, Nat. Biomed. Eng. 4 (2020) 1053–1062.

[26] S.A. Gaballa, U.B. Kompella, O. Elgarhy, A.M. Alqahtani, B. Pierscionek, R. G. Alany, H. Abdelkader, Corticosteroids in ophthalmology: drug delivery innovations, pharmacology, clinical applications, and future perspectives, Drug Delivery Transl. Res. 11 (2021) 866–893.

[27] Yang, Y.; Lockwood, A. Topical ocular drug delivery systems: innovations for an unmet need. Exp. Eye Res. 2022, 109006.

[28] H. Kang, J.G. Rho, C. Kim, H. Tak, H. Lee, E. Ji, S. Ahn, A.-R. Shin, H.-I. Cho, Y. H. Huh, The miR-24-3p/p130Cas: a novel axis regulating the migration and invasion of cancer cells, Sci. Rep. 7 (2017) 1–10.

[29] G. Yu, Z. Jia, Z. Dou, miR-24-3p regulates bladder cancer cell proliferation, migration, invasion and autophagy by targeting DEDD, Oncol. Rep. 37 (2017) 1123–1131.

[30] H. Zhang, Y. Shi, J. Liu, H. Wang, P. Wang, Z. Wu, L. Li, L. Gu, P. Cao, G. Wang, Cancer-associated fibroblast-derived exosomal microRNA-24-3p enhances colon cancer cell resistance to MTX by down-regulating CDX2/HEPH axis, J. Cell Mol. Med. 25 (2021) 3699–3713.

[31] P. Rahimi, V.I. Mobarakeh, S. Kamalzare, F. SajadianFard, R. Vahabpour, R. Zabihollahi, Comparison of transfection efficiency of polymer-based and lipid-based transfection reagents, Bratisl. Lek. Listy 119 (2018) 701–705.

[32] J.A. Zamora-Justo, P. Abrica-González, G.R. Vázquez-Martínez, A. Muñoz-Diosdado, J.A. Balderas-López, M. Ibáñez-Hernández, Polyethylene glycol-coated gold nanoparticles as DNA and atorvastatin delivery systems and cytotoxicity evaluation, J. Nanomater. 2019 (2019), 5982047.

[33] H.L. Chandler, T. Tan, C. Yang, A.J. Gemensky-Metzler, R.F. Wehrman, Q. Jiang, C. M. Peterson, B. Geng, X. Zhou, Q. Wang, D. Kaili, T.M.A. Adesanya, F. Yi, H. Zhu, J. Ma, MG53 promotes corneal wound healing and mitigates fibrotic remodeling in rodents, Commun. Biol. 2 (2019) 1–10.

[34] A.V. Ljubimov, M. Saghizadeh, Progress in corneal wound healing, Prog. Retin. Eye Res. 49 (2015) 17–45.

[35] Q. Tang, B. Lu, J. He, X. Chen, Q. Fu, H. Han, C. Luo, H. Yin, Z. Qin, D. Lyu, Exosomes-loaded thermosensitive hydrogels for corneal epithelium and stroma regeneration, Biomaterials 280 (2022), 121320.

[36] G.M. Fernandes-Cunha, K.-S. Na, I. Putra, H.J. Lee, S. Hull, Y.-C. Cheng, I.J. Blanco, M. Eslani, A.R. Djalilian, D. Myung, Corneal wound healing effects of mesenchymal stem cell secretome delivered within a viscoelastic gel carrier, Stem Cells Transl. Med. 8 (2019) 478–489.

[37] K.Y. Han, J.A. Tran, J.H. Chang, D.T. Azar, J.D. Zieske, Potential role of corneal epithelial cell-derived exosomes in corneal wound healing and neovascularization, Sci. Rep. 7 (2017) 1–14.

[38] M.K. Reumann, C. Linnemann, R.H. Aspera-Werz, S. Arnold, M. Held, C. Seeliger, A.K. Nussler, S. Ehnert, Donor site location is critical for proliferation, stem cell capacity, and osteogenic differentiation of adipose mesenchymal stem/stromal cells: implications for bone tissue engineering. Int, J. Mol. Sci. 19 (2018) 1868.

[39] Y. Zhu, T. Liu, K. Song, X. Fan, X. Ma, F. Cui, Adipose-derived stem cell: a better stem cell than BMSC, Cell Biochem. Funct. 26 (2008) 664–675.

[40] L. Yan, J. Ma, Y. Zhu, J. Zan, Z. Wang, L. Ling, Q. Li, J. Lv, S. Qi, Y. Cao, MiR-24-3p promotes cell migration and proliferation in lung cancer by targeting SOX7, J. Cell. Biochem. 119 (2018) 3989–3998.

[41] Y. Xie, N. Su, J. Yang, Q. Tan, S. Huang, M. Jin, Z. Ni, B. Zhang, D. Zhang, F. Luo, FGF/FGFR signaling in health and disease, Signal Transduct. Targeted Ther. 5 (2020) 1–38.

[42] M. Zakrzewska, L. Opalinski, E.M. Haugsten, J. Otlewski, A. Wiedlocha, Crosstalk between p38 and Erk 1/2 in downregulation of FGF1-induced signaling, Int. J. Mol. Sci. 20 (2019) 1826.

[43] P. Szybowska, M. Kostas, J. Wesche, E.M. Haugsten, A. Wiedlocha, Negative regulation of FGFR (fibroblast growth factor receptor) signaling, Cells 10 (2021) 1342.

[44] D.C. Mitchell, B.A. Bryan, J.-P. Liu, W.-B. Liu, L. Zhang, J. Qu, X. Zhou, M. Liu, D. W. Li, Developmental expression of three small GTPases in the mouse eye, Mol. Vis. 13 (2007) 1144–1153.

[45] S. Muñoz-Descalzo, A. Gomez-Cabrero, M. Mlodzik, N. Paricio, Analysis of the role of the Rac/Cdc42 GTPases during planar cell polarity generation in Drosophila, Int. J. Dev. Biol. 51 (2007) 379–388.

[46] S. Pothula, H.E. Bazan, G. Chandrasekher, Regulation of Cdc42 expression and signaling is critical for promoting corneal epithelial wound healing, Invest. Ophthalmol. Vis. Sci. 54 (2013) 5343–5352.

[47] B. Laviña, M. Castro, C. Niaudet, B. Cruys, A. Álvarez-Aznar, P. Carmeliet, K. Bentley, C. Brakebusch, C. Betsholtz, K. Gaengel, Defective endothelial cell migration in the absence of Cdc42 leads to capillary-venous malformations, Development 145 (2018) dev161182.

[48] L. Xi, Pigment epithelium-derived factor as a possible treatment agent for choroidal neovascularization, Oxid. Med. Cell. Longev. 2020 (2020), 8941057.

[49] R. Mietzner, M. Breunig, Causative glaucoma treatment: promising targets and delivery systems, Drug Discov. Today 24 (2019) 1606–1613.

[50] M.L. Khaled, Y. Bykhovskaya, S.E. Yablonski, H. Li, M.D. Drewry, I.F. Aboobakar, A. Estes, X.R. Gao, W.D. Stamer, H. Xu, Differential expression of coding and long noncoding RNAs in keratoconus-affected corneas, Invest. Ophthalmol. Vis. Sci. 59 (2018) 2717–2728.

[51] M. Ziaei, C. Greene, C.R. Green, Wound healing in the eye: therapeutic prospects, Adv. Drug Deliv. Rev. 126 (2018) 162–176.

[52] G.K. Marino, M.R. Santhiago, A.A.M. Torricelli, A. Santhanam, S.E. Wilson, Corneal molecular and cellular biology for the refractive surgeon: the critical role of the epithelial basement membrane, J. Refract. Surg. 32 (2016) 118–125.

[53] M. Ciano, P.R. Kemp, S.A. Sathyapala, S.M. Hughes, Haploinsufficient maternal effect of epidermal growth factor receptor A mutation in zebrafish, bioRxiv (2019), https://doi.org/10.1101/745018.

[54] K. Shanmugapriya, H. Kim, H.W. Kang, EGFR-conjugated hydrogel accelerates wound healing on ulcer-induced burn wounds by targeting collagen and inflammatory cells using photoimmunomodulatory inhibition, Mater. Sci. Eng., C 118 (2021), 111541.

[55] E.C. Jamerson, A.M. Elhusseiny, R.H. ElSheikh, T.K. Eleiwa, Y.M. El Sayed, Role of matrix metalloproteinase 9 in ocular surface disorders, Eye Contact Lens 46 (2020) S57–S63.

[56] C.M. Kumar, H. Eid, C. Dodds, Sub-Tenon's anaesthesia: complications and their prevention, Eye 25 (2011) 694–703.

[57] D.J.L. Bunker, R.J. George, A. Kleinschmidt, R.J. Kumar, P. Maitz, Alkali-related ocular burns: a case series and review, J. Burn Care Res. 35 (2014) 261–268.